Preparation of Electrospun Porous Alumina Nanofibers for Origami-Inspired Manufacturing

Yu Ni, Ankur Gupta, Gulshan Verma, Sparsh Gupta, Peter G. Weidler, Dario Mager, Jan G. Korvink,* and Monsur Islam*

This article presents the fabrication of 3D shapes of alumina nanofibril sheets using origami-inspired manufacturing. The fabrication process includes electrospinning of a composite precursor material for obtaining a nanofibril mat, which is shaped into 3D origami shapes using a sandwich method during a stabilization process. The 3D origami-shaped precursor nanofibril sheet is calcinated at a high temperature to obtain the 3D origami shapes of alumina nanofibers. It is found that the pre-calcination stabilization process plays a major role in determining the morphology of the resulting alumina nanofibers. A hot plate stabilization process leads to the formation of hollow alumina nanofibers during the calcination step, whereas oven stabilization results in a porous morphology of the alumina nanofibers. The oven stabilization is favorable for the origami alumina structures, as it allows uniform stabilization conditions. The alumina nanofibers are majorly mesoporous and feature a surface area ranging from 118 to 505 m^2g^{-1}. The compressive modulus of the alumina nanofibers exhibits a dependence on the precursor concentration and calcination temperature. The 3D origami structures of alumina nanofibers exhibit excellent structural stability at high temperatures. The high porosity and high-temperature stability position alumina origami shapes as suitable candidates in many high-temperature applications.

1. Introduction

Origami is an ancient Japanese art of paper folding, widely used for decoration and aesthetic purposes worldwide. Traditionally, 3D origami shapes are achieved by folding a 2D flat sheet of paper along prescribed crease lines. In recent years, origami has been attracting significant interest from the scientific community since it has the ability to produce a wide variety of sophisticated architectural shapes despite low processing costs and no requirement for complex infrastructure. Furthermore, the choice of materials for origami has been expanded beyond traditional paper-based substrates. Our previous publications demonstrated the origami folding of carbon sheets through the carbonization of a folded origami-shaped polymeric precursor sheet.[1–3] These origami structures exhibited high mechanical stiffness at a low structural density, which is advantageously comparable to other lightweight materials, including carbon nanotube form, graphene elastomer, metallic nanolattices, and silica aerogel. Furthermore, infiltration of the folded precursor sheet with a metal precursor, followed by high-temperature pyrolysis, led to the fabrication of metal carbide origami shapes.[4,5] Origami folding of refractory ceramic materials is yet to be achieved. Here, we expand the material library of origami folding to alumina material as an ideal refractory material.

Alumina (Al_2O_3) is one of the most popular refractory ceramic materials due to its interesting intrinsic properties, including high thermal resistance, excellent chemical resistant, electrical insulation, high mechanical properties, and good biocompatibility.[6–8] These properties have enabled alumina as one of the preferred materials in several applications, including structural components in high-temperature applications, heat engine and aerospace applications, electronic substrates, and biomedical applications.[9–11] Recent progress

Y. Ni, D. Mager, J. G. Korvink, M. Islam
Institute of Microstructure Technology
Karlsruhe Institute of Technology
Hermann-von-Helmholtz-Platz 1, 76344 Eggenstein-Leopoldshafen
Germany
E-mail: jan.korvink@kit.edu; monsur.islam@kit.edu

A. Gupta, G. Verma
Department of Mechanical Engineering
Indian Institute of Technology
Jodhpur 342037, India

S. Gupta
Mechanical Engineering Department
Punjab Engineering College
Sector 12, Chandigarh 160012, India

P. G. Weidler
Institut für Funktionelle Grenzflächen
Karlsruhe Institute of Technology
Hermann-von-Helmholtz-Platz 1, 76344 Eggenstein-Leopoldshafen
Germany

The ORCID identification number(s) for the author(s) of this article can be found under https://doi.org/10.1002/adem.202201183.

in nanotechnology has enabled the nanostructuring of alumina in different 1D structures, such as nanofibers and nanorods.[12–14] However, the assembly of these nanostructured alumina into 3D complex shapes is still a major challenge. In fact, 3D shaping of alumina predominantly relies on the casting method, which restricts the transformation into complex shapes due to the lack of design freedom and costly mold fabrication. In the past two decades, rapid progress in additive manufacturing technologies has also enabled the 3D printing of alumina materials, which has allowed the fabrication of numerous complex 3D shapes due to its wide design freedom. Typically, an alumina slurry is extruded,[15,16] or an alumina nanoparticle-based photoactive resin is photocured using a UV source to achieve the complex 3D shapes. Deriving 3D alumina from the 3D printed shapes with these methods requires a long (up to a few days) debinding and sintering process. Furthermore, the 3D printable slurry preparation often requires complex chemistry, making the entire process quite sophisticated. Here, we postulate origami-inspired manufacturing as a facile approach for fabricating 3D complex shapes of alumina by integrating electrospinning and paper-folding methods.

The properties of a cellular structure depend on the constituent material, geometrical feature, and its microstructure.[17,18] To date, origami patterning has been achieved using sheets featuring either solid film or microfibril microstructures. Nanostructural microstructure has proved to exhibit superior properties in several 3D cellular architectures.[19] Electrospinning is a well-known technique for producing nanofibers with a fiber diameter ranging from a few nanometers to a few microns. Due to the nanoscale 1D nature, electrospun fibers feature several unique properties, high specific surface area, tunable porosity, high mechanical properties, and high chemical and thermal stability.[20,21] These properties have enabled electrospun nanofibers in a plethora of applications, including energy harvesting, tissue engineering, filtration, food packaging, and environmental remediation, to name a few.[21–27] Furthermore, electrospinning allows for deriving nanofibers of many different materials beyond polymers, such as carbon, metal oxides, metal carbides, metal–organic frameworks, and perovskite materials.[28–31] The feasibility of electrospinning of alumina, which is of interest in this work, has also been demonstrated a few times by other researchers.[32–35] These electrospun alumina nanofibers featured high porosity, which enabled their use in several applications, including catalyst support, chemical adsorption, particulate filtration, pollutant removal, and water treatment.[33,36–38] However, no 3D structuring of these alumina nanofibers has been reported to date.

Considering the advantages of electrospun alumina nanofibers stated earlier, electrospinning is chosen here for preparing the sheet that can result in an origami structure with nanometric microstructure. In this work, alumina nanofibers are prepared by electrospinning a composite precursor solution, followed by stabilization and calcination. We first characterize the morphology and material properties of electrospun alumina nanofibers based on the precursor configuration and thermal treatment conditions. Origami folding of alumina nanofibril sheets is demonstrated using a facile sandwich-mode approach. Of note, this is, to the best of the authors' knowledge, the first demonstration of origami folding of alumina nanofiber sheets. In fact, this work also demonstrates for the first time the origami folding of electrospun nanofibers as well as oxide ceramics. It should also be noted that this work only focuses on the demonstration of origami foldability of electrospun alumina nanofibers. The properties arising due to the nanofibril constituent are not studied here.

2. Results and Discussion

Electrospinning of a polyacrylonitrile (PAN)/aluminum acetylacetonate composite solution with different concentrations of aluminum acetylacetonate was performed using the parameters mentioned in the experimental section. The average diameter of the electrospun composite fibers was 1048 ± 288 nm. The electrospun fibers underwent a stabilization process before calcination. Two approaches were used for stabilization. The first approach used heat treatment at 250 °C for 2 h within an oven for stabilization. The second approach used a hot plate heating at 200 °C for 2 h. During calcination, the polymeric counterpart of the electrospun fibers was completely removed through oxidation, whereas aluminum acetylacetonate was oxidized to form alumina.[39,40] The calcination temperature was varied from 800 to 1200 °C to obtain alumina nanofibers.

2.1. Effect of Stabilization Process on the Morphology of Alumina Fibers

The stabilization process exhibited a strong impact on the morphology of the final alumina nanofibers. **Figure 1** shows the alumina nanofibers for different Al precursor concentrations and different calcination temperatures, when stabilized in the oven. It can be observed that the oven-stabilized nanofibers featured a porous morphology for all the calcination temperatures for 5% and 10% Al precursor concentrations. The porosity seemed to increase with the calcination temperature, as distinctive and uniformly distributed pores were observed in the nanofibers for 1200 °C, as shown in Figure 1c,f. Alumina nanofibers with a 15% concentration exhibited different morphological features. At 800 °C, the nanofibers were highly porous (Figure 1g), similar to other concentrations. However, as the calcination temperature increased, the morphology gradually transformed into hollow nanofibers. For instance, the nanofibers obtained at 1000 °C seemed to feature less porosity compared to the one obtained at 800 °C, but they started forming shells with porous substances at the core, forming a semi-hollow morphology (Figure 1h). The calcination temperature of 1200 °C resulted in completely hollow nanofibers, as shown in Figure 1h, where the cross-sectional view of the nanofibers (inset of Figure 1h) gives direct evidence for it. The wall thickness of these hollow nanofibers was 15 ± 4 nm.

In contrast to the oven-stabilized nanofibers, hot-plate stabilization resulted in hollow nanofibers, regardless of the precursor concentration and calcination temperature, as presented in **Figure 2**. The wall thickness of these hollow nanofibers ranged from 10 to 30 nm. However, no correlation was found between the wall thickness of these hollow nanofibers and the Al precursor concentration and calcination temperature. The morphology of these nanofibers exhibited several interesting features. The surface of the hollow nanofibers was not smooth, rather the
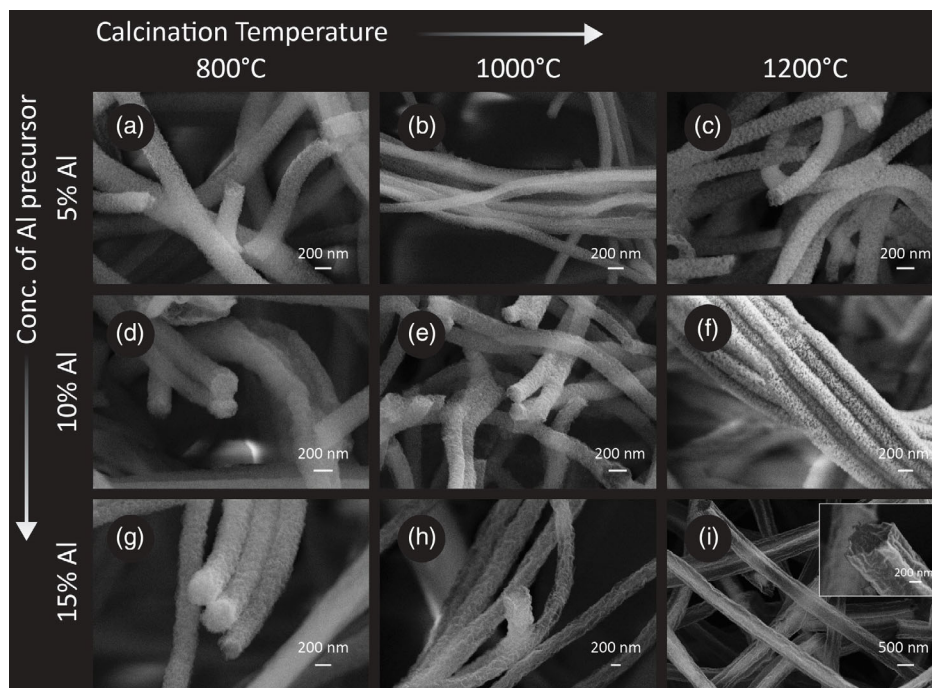
Figure 1. Scanning electron microscopy SEM) images of alumina nanofibers obtained for different Al precursor concentrations and calcination temperatures in case of stabilization in the oven. The nanofibers featured mostly porous microstructure, except h) and i). h) shows a semi-hollow fiber, whereas i) shows a completely hollow feature. Inset of (i) shows the cross-section of the fibers, emphasizing the hollow feature.
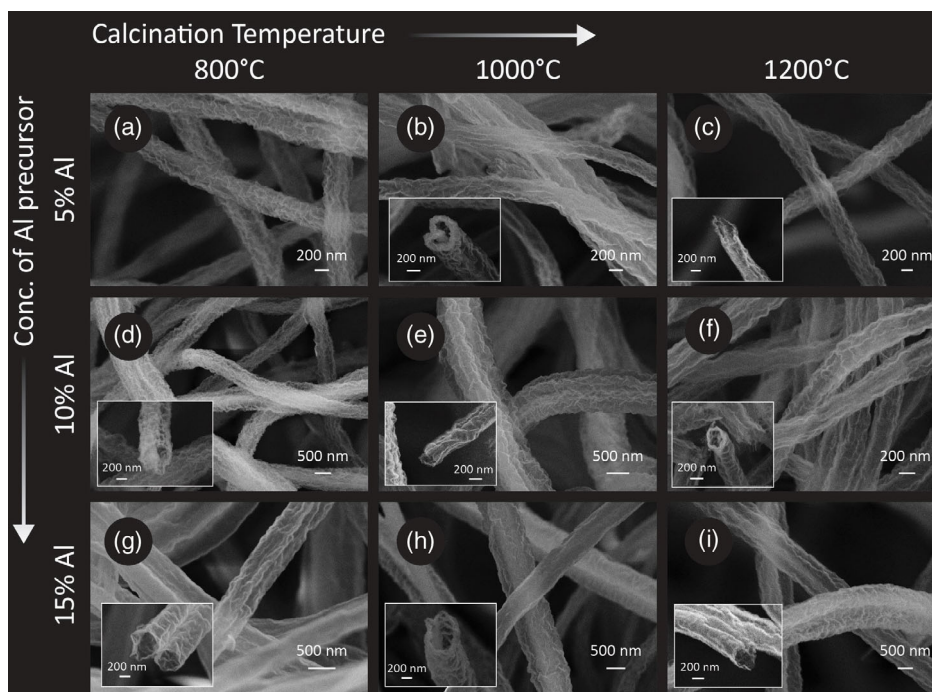

Figure 2. SEM images of alumina nanofibers obtained for different Al precursor concentrations and calcination temperatures in case of stabilization on a hot plate. Note that all the nanofibers feature hollow microstructures. The insets of the figures show the cross-sections of the respective fibers, emphasizing the hollow features.

nanofibers featured wrinkled surfaces. In several instances, adjacent nanofibers seemed to fuse together during calcination to result in a single hollow nanofiber. Examples of such are shown in the insets of Figure 2b,d.
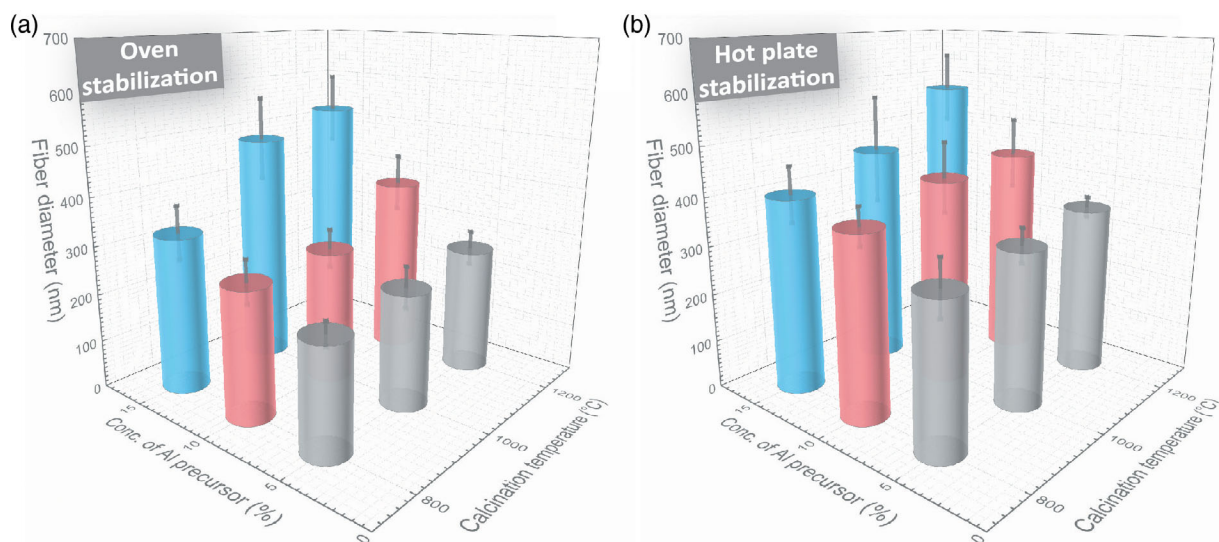
**ADVANCED
SCIENCE NEWS**

www.advancedsciencenews.com

**ADVANCED
ENGINEERING
MATERIALS**

www.aem-journal.com

Figure 3. Distribution of alumina nanofiber diameter based on calcination temperature and aluminum precursor concentration for: a) oven stabilization and b) hot plate stabilization.

The stabilization approach also impacted the fiber diameters. Figures S2 and S3, Supporting Information present the fiber size distributions for oven-based stabilization and hot plate stabilization, respectively. The average fiber diameters are plotted in **Figure 3**a,b, respectively. For comparison, both the figures featured the same range in Z-axis. It can be observed that in both cases, fiber diameter increased with the calcination temperature and the concentration of Al precursor. However, the impact of Al precursor concentration was significantly stronger than the calcination temperature. For example, in the case of oven stabilization of 15% Al precursor concentration, fiber diameter increased from 325 ± 56 nm for 800 °C to 525 ± 73 nm for 1200 °C, resulting in an increment of 62% in fiber diameter. In comparison, for 1200 °C calcination temperature, an increase in Al precursor concentration from 5% to 15% resulted in an increase in fiber diameter from 262 ± 36 to 525 ± 73 nm, leading to a $\approx$100% increase in fiber diameter. The hot-plate stabilization resulted in relatively larger fiber diameters compared to oven stabilization. For example, the increase of precursor concentration from 5% to 15% at 1200 °C yielded an increase in the fiber diameter from 352 ± 21 to 574 ± 73 nm.

The stabilization method had a significant impact on the morphology and dimensions of the resulting alumina nanofibers, as discussed in the previous paragraphs. Here we propose a mechanism for such dependency on the stabilization process, which is schematically presented in **Figure 4**. The formation of porous or hollow nanofibers can be explained by the crystal diffusion mechanism. Hot plate heating resulted in a local thermal gradient due to heat convection and radiation, which might have triggered the movement of aluminum acetylacetonate nanoparticles from the core of the fibers to the surface, making the surface aluminum-richer than the core. During calcination, the aluminum-rich surface might have started to get oxidized first, converting surface aluminum acetylacetonate to alumina nucleation sites. The surface alumina further resulted in oxygen deficiency for the

aluminum acetylacetonate in the core. Therefore, the concentration gradient from the core to the surface led the aluminum acetylacetonate diffuse to the surface. Furthermore, aluminum acetylacetonate has a significantly lower melting temperature than alumina. The melting temperature of aluminum acetylacetonate is $\approx$192 °C, whereas alumina has a melting temperature of $\approx$2072 °C. Therefore, following the Kirkendall effect, the diffusion rate of aluminum acetylacetonate is much faster than alumina.[39,41] The faster diffusion rate of aluminum acetylacetonate toward the surface results in hollow voids at the core. The aluminum acetylacetonate further gets oxidized to form alumina during calcination, whereas the host PAN matrix completely gets removed during oxidation, resulting in hollow nanofibers.

In contrast to the hot plate, the oven provides uniform heat conditions. Therefore, during stabilization inside an oven, the precursor nanofibers did not experience a thermal gradient. Rather, the aluminum acetylacetonate within the PAN matrix might have homogeneously cross-linked to the polymeric chains of PAN, which further restricted the diffusion of the aluminum acetylacetonate to the surface during calcination. Such lack of diffusion led to in situ oxidation of the aluminum acetylacetonate to form alumina crystallites. The complete oxidation of the polymeric matrix further led to the porous morphology of the resulting alumina nanofibers, as shown in Figure 4a. For higher calcination temperatures ($>$1000 °C), the resulting γ-alumina started transforming to α-alumina (see Section 2.2). The phase transformation initiated another phase-separation-induced crystal diffusion, which further led to hollow morphology for the nanofibers obtained at 1200 °C, even for oven stabilization.

As the final goal of the work was to achieve origami-inspired manufacturing of alumina nanofibers, it was important to achieve a nanofiber sheet with uniform properties. Oven stabilization yielded more uniform behavior compared to hot plate stabilization, which can be depicted by the relatively smaller
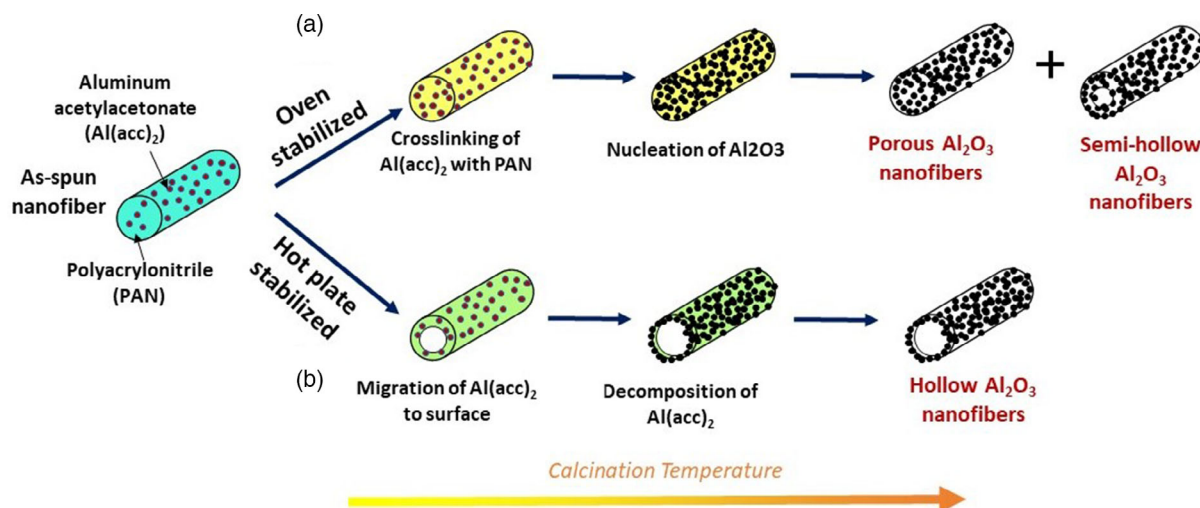
Figure 4. Schematic illustration of the formation of porous and hollow alumina nanofibers for: a) oven stabilization and b) hot plate stabilization.

standard deviation in the fiber diameter in case of oven stabilization as shown in Figure 3. Furthermore, oven stabilization provided better cross-linking to the as-spun fibers, leading to better rigidity in the folded sheets within the mold origami structures. Therefore, further characterization was performed only for the oven-stabilized nanofibers.

2.2. Effect of Precursor Concentration and Calcination Temperature on the Composition of Alumina Nanofibers

Figure 5 presents the X-ray diffraction (XRD) diffraction patterns of alumina nanofibers synthesized at different Al precursor concentrations and calcination temperatures. For all the three precursor concentrations, the calcination temperature of 800 °C resulted in broad peaks around 31.8°, 36.8°, 45.8°, and 67.1° in their XRD diffractograms (Figure 5a–c), which correspond to (220), (311), (400), and (440) crystal planes of γ-Al_2O_3 and match to the PDF number 10-0425 in International Centre for Diffraction Data (ICDD) database.[42] In addition to these XRD peaks, another broad peak around 61.1° appeared for the samples obtained at the calcination temperature of 1000 °C, which corresponds to the (511) plane. Furthermore, the peaks were sharper for 1000 °C calcination temperature, compared to 800 °C, which suggests enhanced crystallinity of γ-Al_2O_3 for increased calcination temperature. Unlike the XRD patterns of 800 and 1000 °C, no peaks of γ-Al_2O_3 was observed in the XRD diffractograms of the samples calcined at 1200 °C (Figure 5a–d). The peaks in the XRD patterns for 1200 °C were indexed to α-Al_2O_3 and matched to ICDD PDF number 46-1212.[43] This suggested that increasing the calcination temperature from 1000 to 1200 °C resulted in the transformation of γ-Al_2O_3 to α-Al_2O_3. Such high-temperature phase transformations are in agreement with previous publications.[44–46] We further compared the XRD diffractograms of 1200 °C calcined samples for different Al precursor concentrations in Figure 5d. Even though all the concentrations resulted in the formation of α-Al_2O_3, the peak intensities increased with the increase in Al precursor concentration. This infers that the higher

concentration of Al precursor yielded higher relatively higher crystallinity of the resulting α-Al_2O_3.

2.3. Porosity of the Alumina Nanofibers

Figure 6 displays the argon adsorption and desorption isotherms as well as the related pore size distribution of the alumina nanofibers with 5 to 15 wt% Al precursor concentrations. All the samples exhibited the type IV adsorption isotherms (Figure 6a), where the existence of mesoporous structures is indicated by a significant increase in adsorption volume at $P/P_0 = 0.8$–1.0.[35] The samples with 5, 10, and 15 wt% Al precursor nanofibers had corresponding surface areas of 118, 505, and 126 m^2g^{-1}, respectively, while calculating using DFT methods. The DFT pore size distribution graphs of the alumina nanofibers are shown in Figure 6b. The mean pore diameters of the alumina nanofibers with 5, 10, and 15 wt% Al precursor concentrations were ≈9 nm, 9 to 16 nm, and 7 nm, respectively. The results emphasized the mesoporous nature of the alumina nanofibers.

2.4. Mechanical Properties of the Alumina Nanofibers

The mechanical properties of the alumina nanofibers were evaluated by performing compression tests of a composite matrix of alumina nanofibers and polydimethylsiloxane (PDMS) elastomer. The experimental details are provided in the experimental section. **Figure 7** depicts the variation in compression modulus of prepared alumina nanofibers as a function of Al precursor concentration (wt%) and calcination temperature. The compression modulus increased with the calcination temperature, as well as the Al precursor concentration. The fibers obtained at 1200 °C exhibited significantly higher compression modulus compared to the other two calcination temperatures. For example, the compression modulus of the alumina fibers with 5% Al concentration increased from 65.7 ± 28.5 MPa at 800 °C to 151.6 ± 73.3 MPa at 1200 °C, resulting in a 130% increase in the modulus. Such improvement can be attributed to the formation of α-Al_2O_3 at 1200 °C, as evidenced by the XRD
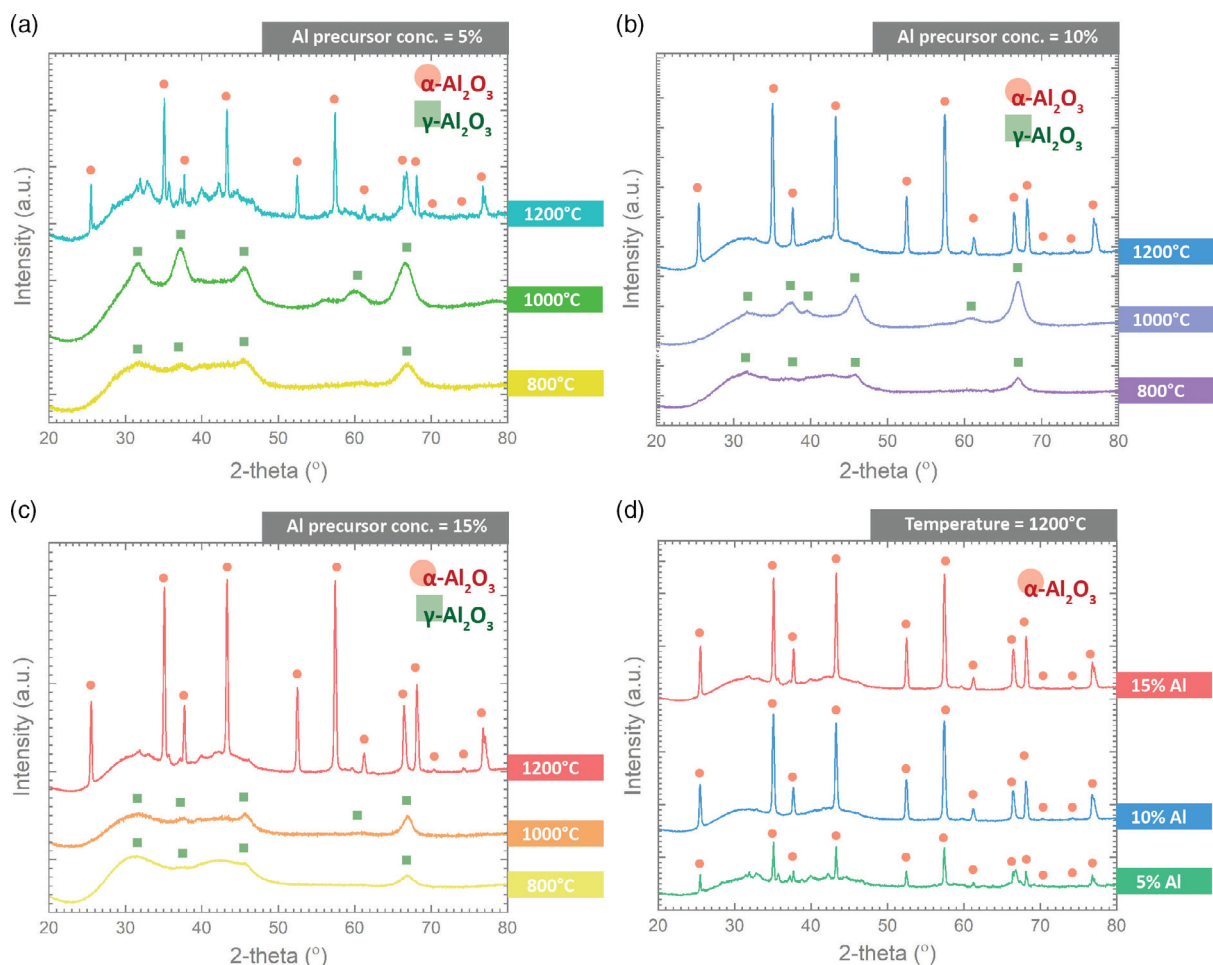
Figure 5. X-ray diffraction (XRD) diffractograms of alumina nanofibers obtained at different calcnination temperatures for Al precursor concentrations of: a) 5%, b) 10%, and c) 15%. d) Comparison of XRD diffractorams of alumina nanofibers obtained at 1200 °C for different Al precursor concentrations.
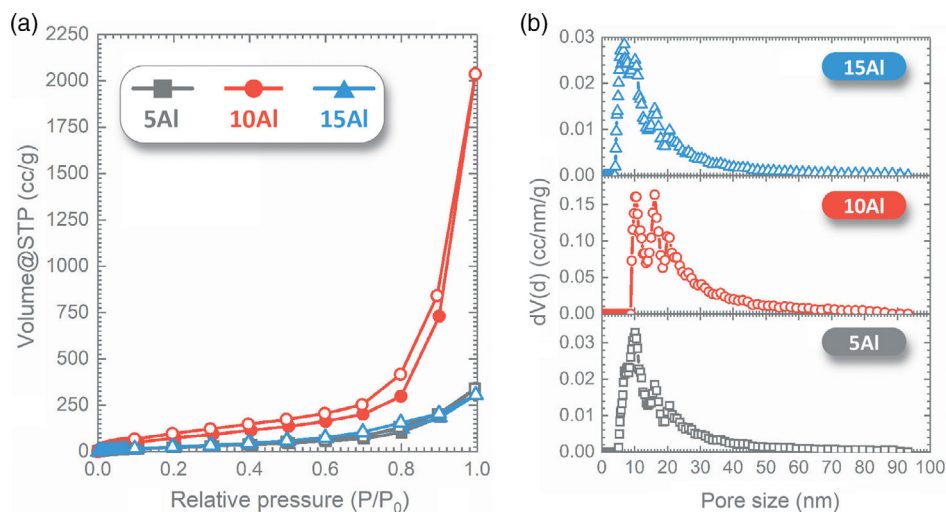

Figure 6. a) Argon adsorption–desorption isotherms and b) pore size distributions of alumina nanofibers for different Al precursor concentrations obtained at 1000 °C calcination temperature.
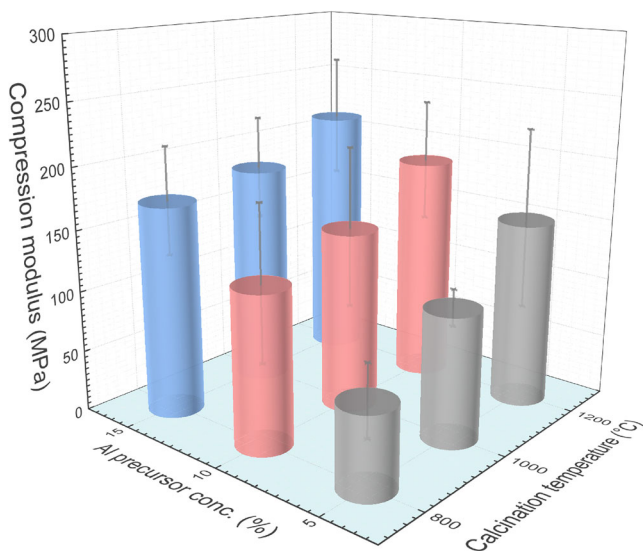
Figure 7. Compression modulus of alumina nanofibers with different Al precursor concentrations and calcination temperatures.

diffractograms (Figure 5).[47] Furthermore, for the calcination temperature of 1200 °C, the increase in the Al concentration resulted in a 16.0% increase in the modulus, from 151.6 ± 73.3 MPa for 5% Al concentration to 212.5 ± 50.5 MPa for 15% Al concentration. Such improvement was expected, as a higher concentration of Al precursor led to a higher amount

of alumina content within the fibers, yielding higher resistance to the compression force. It should be noted here that the standard deviation in the measurements is significantly higher. This could be a result of the inhomogeneity of the orientation and concentration of alumina nanofibers within the PDMS matrix.

2.5. Origami-Patterning of Alumina Nanofibers

We demonstrated the fabrication of origami structures of the electrospun alumina nanofibers. The origami folding is detailed in the Experimental section. Briefly, an electrospun precursor sheet was sandwiched between two-folded paper origami structures, which went through the stabilization process in the oven. Upon stabilization, the paper origami structures were carefully removed to obtain the electrospun precursor structure. The stabilization process ensured that the electrospun sheet retained the origami pattern. Hot plate stabilization could not be implemented here as it does not allow uniform stabilization, particularly in the sandwich mode, due to the poor heat transfer capability of the paper origami. The electrospun origami sheet retained the structural geometry after the calcination step. **Figure 8**a,b shows a folded Yoshimura and a folded Umbrella structure, respectively. In both figures, the left origami structures are the paper mold structure used to fold the electrospun precursor sheets, and the right ones are the alumina origami structures. The significant geometrical shrinkage (up to ≈80%) can be noted in both figures. Figure 8c presents an example of scanning electron microscopy (SEM) images of the alumina origami structure
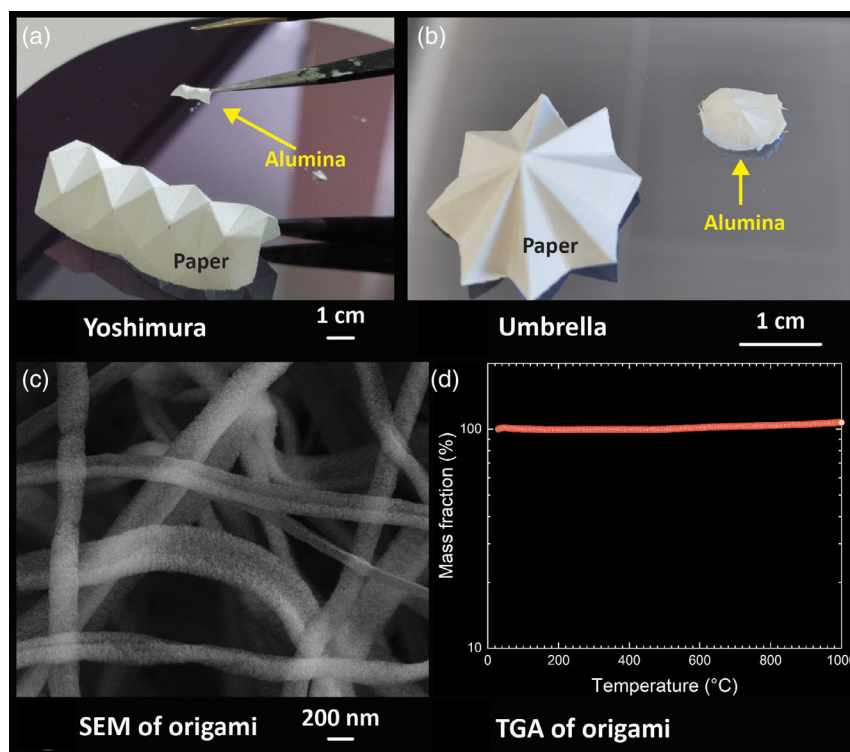

Figure 8. a) Yoshimura and b) Umbrella origami structure. The paper origami structure and resulting alumina origami structures are indicated in the figures. c) SEM image of alumina origami structure, emphasizing the porous nature of the constituent nanofibers. d) Thermogravimetric analysis (TGA) of alumina Yoshimura in air atmosphere, depicting the excellent thermal resistance of the alumina origami structures.

calcinated at 1200 °C, which shows the porous morphology of the nanofibers. Even though Yoshimura and Umbrella origami structures of alumina nanofiber sheets retained the precursor geometry, Miura-ori structures failed. Figure S5, Supporting Information shows the mold paper Miura-ori and the resulting alumina Miura-ori. The alumina Miura-ori featured several cracks and raptures, which were the results of sharp corners of the mold Miura-ori. The asymmetric unit cell geometry of Miura-ori yielded asymmetric shrinkage of the alumina nanofiber sheet, which further contributed to the failure of the alumina Miura-ori. Increasing the nanofibril sheet thickness may solve this issue. The thicker film provides higher rigidity, which can endure the shrinkage of the geometry during calcination and further be minimally affected by the sharp features of mold paper geometry. A detailed study is needed to evaluate such aspects. Our current efforts include investigating these parameters influencing the structural rigidity of alumina origami structures and fabricating different complex origami geometry.

The results of origami folding are promising. Such alumina origami structures hold a huge promise in several applications. Alumina is a refractory material and can withstand extremely high working temperatures. Therefore, alumina origami structures can be used for high-temperature applications. To test the high-temperature applicability of the origami structures, we performed thermogravimetric analysis (TGA) of an alumina Yoshimura origami structure up to 1000 °C in an air atmosphere. The TGA result of the alumina Yoshimura is presented in Figure 8d. As expected, no weight loss was observed in the TGA curve. Rather, after ≈500 °C, a slight weight gain was observed, possibly due to the entrapping of hot air within the pores. Such high-temperature resistance of alumina origami structures can also be utilized in several high-temperature applications, including high-temperature filters for gas separation and high-temperature structural materials. Furthermore, the highly porous nature of the alumina nanofibers makes the origami patterns lightweight. Due to the nanofibril microstructure and their high mechanical properties, alumina origami structures are expected to exhibit high mechanical stiffness and strength at a low density. However, these mechanical properties of alumina origami are yet to be investigated. A detailed and methodical study is needed to validate these claims.

3. Conclusion

In this article, we have demonstrated, for the first time, origami-inspired manufacturing of electrospun alumina nanofibers. The alumina nanofibers were first studied for their morphology. The nanofibers were prepared using electrospinning of an aluminum acetylacetonate/PAN composite solution, followed by a stabilization step and the subsequent high-temperature calcination step. We found that the stabilization process was the major factor in determining the morphology of the resulting alumina nanofibers. A hot plate stabilization process led to the formation of hollow alumina nanofibers during the calcination step, whereas oven stabilization resulted in the porous morphology of the nanofibers. Furthermore, the composition and dimension of the nanofibers exhibited a strong dependence on the calcination temperatures and Al precursor concentration. The alumina

nanofibers featured majorly mesoporous microstructure, resulting in a high surface area. Furthermore, they exhibited high compression modulus under compression tests. Origami structures of alumina nanofibers were obtained using a sandwich fabrication process. The porous nanofibers were chosen for origami folding due to uniform stabilization and molding conditions. Even though Yoshimura and Umbrella origami structures were successfully fabricated using the sandwich method, Miura-ori patterns failed. More studies are needed to fold alumina nanofibers to successfully yield complex structures like Miura-ori. Nevertheless, the origami structures showed high-temperature resistance due to the inherent thermal inertness of alumina nanofibers. These results are promising for achieving structural shapes of alumina nanofibers for high-temperature applications.

4. Experimental Section

Material: PAN (average $Mw = 150\,000$), N,N Dimethylformamide (DMF), and aluminum acetylacetonate (Aluminum 2,4-pentanedionate) were from Sigma Aldrich, Germany. All raw materials were used as received.

Preparation of Alumina Nanofibers: To prepare the electrospinnable precursor solution, a 10 wt% PAN solution was prepared in DMF on a magnetic stirred overnight at 50 °C. Afterward, aluminum acetylacetonate was added to the PAN/DMF solution to achieve an aluminum acetylacetonate concentration of 5%, 10%, or 15% and the mixed solution was stirred for 1 h at room temperature. The precursor solution was transferred into a 1 mL plastic syringe and electrospun using a custom-built electrospinning setup using the following parameters: applied voltage = 18 kV, distance between needle to collector plate = 13 cm, flow rate = 20 μL min⁻¹.

The electrospun samples were stabilized before calcination. Two different approaches were employed for the stabilization. In the first approach, the stabilization was performed in an oven at 250 °C for 2 h. The second approach used a hot plate heating at 250 °C for 2 h for the stabilization process. Upon stabilization, the electrospun fibers were calcinated in a tube furnace (Carbolite Giro, Germany) to obtain alumina nanofibers. The calcination protocol involved three steps: i) heating from room temperature to the final calcination temperature using a heating ramp of 5 °C min⁻¹, ii) dwelling for 2 h at the final calcination temperature, and iii) cooling down to room temperature using natural cooling. Final calcination temperatures of 800, 1000, and 1200 °C were investigated here.

Characterization of Electrospun Alumina Nanofibers: The alumina nanofibers obtained after calcination were characterized for their morphological features under SEM (Carl Zeiss AG—SUPRA 60VP SEM). The SEM images were analyzed by ImageJ software to obtain average diameter and standard deviation in measurement. XRD was performed on Bruker D8 Advance diffractometer using Cu-Kα radiation ($\lambda = 1.5405$ Å) to determine the specific materials obtained after calcination. The porosity of alumina nanofibers was determined by measuring the argon adsorption–desorption at 87 K using a Quantachrome Autosorb–1 MP gas sorption analyzer (Quantachorme Instruments, USA). The specific surface area, pore volume, and pore size of the samples were measured using density functional theory (DFT) model.[48,49] TGA of alumina origami structures up to 1000 °C was performed in a STARe System TGA/DSC 3+ system in an air atmosphere.

Mechanical Properties of Alumina Nanofibers: The mechanical properties of the alumina nanofibers were characterized using a compression test. However, the alumina nanofibers sheets were extremely challenging to handle for compression tests due to their nanofibril nature. To facilitate the compression test, a composite of alumina nanofibers and PDMS was prepared. Liquid PDMS was first prepared by mixing Sylgard 184 silicone elastomer with the curing agent in a 10:1 (wt.) ratio, followed by degassing in a desiccator for 2 h. To the liquid PDMS, alumina nanofibers were dispersed using mechanical stirring for another 1 h. The composite mixture was poured into a cylinder mold of PMMA sheet, which was again

degassed and finally cured on a hot plate at 95 °C for 5 h. The cured PDMS/alumina structures were detached from the mold and prepared for compression tests. A pure PDMS test structure was also used as a reference for the compression tests. The compression test was performed following the ASTM D575 Test by using Zwick Roell tensile testing machine, using a 140 N load cell, and with a compression rate of 1 mm min^{-1}. Examples of stress–strain curves obtained from the compression tests are presented in Figure S4, Supporting Information. The compressive stress continued increasing with compressive strain, which is typical for PDMS-based materials due to their elastomeric nature.[50,51] The compression modulus of the composite structure ($E_{composite}$) was calculated from the slope of the stress–strain curve. The compression modulus of PDMS (E_{PDMS}) was calculated first by the compression test of the pure PDMS structure. The compression modulus of alumina nanofibers ($E_{alumina}$) was calculated using Equation (1), where m is the mass fraction of PDMS in the composite.

$$E_{composite} = mE_{PDMS} + (1 - m)E_{alumina} \tag{1}$$

Origami Folding of Alumina Nanofibers: The origami patterning of alumina nanofibers was achieved through a replication process through sandwich mode. The process flow is presented in Figure S1, Supporting Information. A mold paper origami pattern was first fabricated. Details of the paper folding are reported in previous publications.[3] The process started with designing the crease patterns using Solidworks (Dassault Systems, Waltham, MA, USA). Three patterns were chosen for the demonstration, which were umbrella, Yoshimura, and Miura-ori. Next, the crease lines were engraved on a Whatman 3MM Grade 1 Chr Cellulose Chromatography Paper (CAT No. 3001-861) using a CO_2 laser engraver machine (ULS Versa Laser 3.50, wavelength: 10.6 µm, lens 2.0 in., beam diameter 120 µm at focus). The paper was folded manually along the crease lines to obtain 3D paper origami structures. An electrospun precursor fiber mat was sandwiched between two paper origami structures and stabilized at 250 °C in an oven. The oven stabilization was used to achieve complete stabilization. Upon stabilization, the paper origami structures were removed carefully to obtain the electrospun origami structures, which were further calcinated at 1200 °C for 2 h to obtain the origami structures of alumina nanofibers.

Supporting Information

Supporting Information is available from the Wiley Online Library or from the author.

Conflict of Interest

The authors declare no conflict of interest.

Data Availability Statement

The data that support the findings of this study are available on request from the corresponding author. The data are not publicly available due to privacy or ethical restrictions.

[1] M. Islam, J. Flach, R. Martinez-Duarte, *Carbon* **2018**, *133* 140.

[2] M. Islam, R. Martinez-Duarte, *Mater. Today: Proc.* **2022**, *48*, 16.

[3] M. Islam, P. G. Weidler, D. Mager, J. G. Korvink, R. Martinez-Duarte, *Micromachines* **2022**, *13*, 503.

[4] M. Islam, D. Keck, R. Martinez-Duarte, *Adv. Eng. Mater.* **2019**, *21*, 1900290.

[5] M. Islam, R. Martinez-Duarte, *Materialia* **2020**, *11*, 100734.

[6] P. Auerkari, *Mechanical and Physical Properties of Engineering Alumina Ceramics*, vol. 23, Technical Research Centre of Finland Espoo, Espoo, Finland **1996**.

[7] D. Losic, A. Santos, *Nanoporous Alumina:Fabrication, Structure, Properties and Applications*, Springer, NY, **2015**.

[8] M. Rahmati, M. Mozafari, *J. Cell. Physiol.* **2019**, *234*, 3321.

[9] F. A. Al-Sanabani, A. A. Madfa, N. H. Al-Qudaimi, *Am. J. Mater. Res.* **2014**, *1*, 26.

[10] S. Said, S. Mikhail, M. Riad, *Mater. Sci. Energy Technol.* **2019**, *2*, 288.

[11] A. Ruiz-Clavijo, O. Caballero-Calero, M. Martn-González, *Nanoscale* **2021**, *13*, 2227.

[12] L. Li, X. Liu, G. Wang, Y. Liu, W. Kang, N. Deng, X. Zhuang, X. Zhou, *Chem. Eng. J.* **2021**, *421* 127744.

[13] X. Tang, Y. Yu, *Ceram. Int.* **2015**, *41*, 9232.

[14] J. N. D. de León, V. Petranovskii, A. José, G. Alonso-Nunez, T. A. Zepeda, S. Fuentes, J. L. Garca-Fierro, *Appl. Catal., A* **2014**, *472*, 1.

[15] S. Mamatha, P. Biswas, P. Ramavath, D. Das, R. Johnson, *Ceram. Int.* **2018**, *44*, 19278.

[16] H. Wu, Y. Cheng, W. Liu, R. He, M. Zhou, S. Wu, X. Song, Y. Chen, *Ceram. Int.* **2016**, *42*, 17290.

[17] F. Fernandes, R. Jardin, A. Pereira, R. A. De Sousa, *Mater. Des.* **2015**, *82*, 335.

[18] I. Gibson, M. F. Ashby, *Proc. R. Soc. London. A* **1982**, *382*, 43.

[19] J. Bauer, L. R. Meza, T. A. Schaedler, R. Schwaiger, X. Zheng, L. Valdevit, *Adv. Mater.* **2017**, *29*, 1701850.

[20] B. Zaarour, L. Zhu, X. Jin, *ChemistrySelect* **2020**, *5*, 1335.

[21] B. Zaarour, M. F. Alhinnawi, *J. Ind. Text.* **2022**, *51*, 1S.

[22] B. Zaarour, H. Tina, L. Zhu, X. Jin, *J. Ind. Text.* **2022**, *51*, 1105S.

[23] S. Santangelo, *Appl. Sci.* **2019**, *9*, 1049.

[24] C. Zhang, Y. Li, P. Wang, H. Zhang, *Compr. Rev. Food Sci. Food Saf.* **2020**, *19*, 479.

[25] G. Z. Tan, Y. Zhou, *Int. J. Polym. Mater. Polym. Biomater.* **2020**, *69*, 947.

[26] C. Lyu, P. Zhao, J. Xie, S. Dong, J. Liu, C. Rao, J. Fu, *Nanomaterials* **2021**, *11*, 1501.

[27] M. Wang, K. Wang, Y. Yang, Y. Liu, D.-G. Yu, *Polymers* **2020**, *12*, 103.

[28] M. Islam, C. Dolle, A. Sadaf, P. G. Weidler, B. Sharma, Y. M. Eggeler, D. Mager, J. G. Korvink, *Microsyst. Nanoengin.* **2022**, *8*, 71.

[29] M. Islam, A. D. Lantada, D. Mager, J. G. Korvink, *Adv. Healthcare Mater.* **2022**, *11*, 2101834.

[30] Y. Wang, Y. Jiang, Y. Zhao, X. Ge, Q. Lu, T. Zhang, D. Xie, M. Li, Y. Bu, *Chem. Eng. J.* **2022**, *451*, 138710.

[31] J. Xue, T. Wu, Y. Dai, Y. Xia, *Chem. Rev.* **2019**, *119*, 5298.

[32] P. Panda, S. Ramakrishna, *J. Mater. Sci.* **2007**, *42*, 2189.

[33] Y. Wang, W. Li, X. Jiao, D. Chen, *J. Mater. Chem. A* **2013**, *1*, 10720.

[34] U. Abdillah, H. Yazid, S. Ahmad, S. Makhtar, S. Zaubidah, R. S. Chen, N. Syafiqaz, *IOP Conf. Ser. Mater. Sci. Eng.* **2021**, *1106*, 012019.

[35] J. Shen, Z. Li, Y.-N. Wu, B. Zhang, F. Li, *Chem. Eng. J.* **2015**, *264*, 48.

[36] Y. Wang, W. Li, Y. Xia, X. Jiao, D. Chen, *J. Mater. Chem. A* **2014**, *2*, 15124.

[37] P. Abi Younes, S. Sayegh, A. A. Nada, M. Weber, I. Iatsunskyi, E. Coy, N. Abboud, M. Bechelany, *Colloids Surf., A* **2021**, *628*, 127274.

[38] A. Mahapatra, B. Mishra, G. Hota, *Ind. Eng. Chem. Res.* **2013**, *52*, 1554.

[39] C. Peng, J. Zhang, Z. Xiong, B. Zhao, P. Liu, *Microporous Mesoporous Mater.* **2015**, *215*, 133.

[40] S. Zhou, M. Antonietti, M. Niederberger, *Small* **2007**, *3*, 763.

[41] P. Liu, Y. Zhu, J. Ma, S. Yang, J. Gong, J. Xu, *Colloids Surf., A* **2013**, *436*, 489.

[42] Y. Rozita, R. Brydson, A. Scott, *J. Phys. Conf. Ser.* **2010**, *241*, 012096.

[43] F. R. Feret, D. Roy, C. Boulanger, *Spectrochim. Acta, Part B* **2000**, *55*, 1051.

[44] M. Bodaghi, A. Mirhabibi, H. Zolfonun, M. Tahriri, M. Karimi, *Phase Transitions* **2008**, *81*, 571.

[45] T. C. Chou, T. G. Nieh, *J. Am. Ceram. Soc.* **1991**, *74*, 2270.

[46] S. Lamouri, M. Hamidouche, N. Bouaouadja, H. Belhouchet, V. Garnier, G. Fantozzi, J. F. Trelkat, *Boletn de la Sociedad Española de cerámica y vidrio* **2017**, *56*, 47.

[47] M. Vahtrus, M. Umalas, B. Polyakov, L. Dorogin, R. Saar, M. Tamme, K. Saal, R. Lõhmus, S. Vlassov, *Mater. Character.* **2015**, *107*, 119.

[48] S. Lowell, J. Shields, M. Thomas, M. Thommes, *Characterization Of Porous Solids And Powders: Surface Area, Pore Size And Density*, Springer Verlag, Dordrecht, Netherlands **2006**, iSBN-13-978-1-4020-2303-3 (e-book), p. 347.

[49] J. Landers, G. Gor, A. Neimark, *Colloids Surf. A* **2013**, *437*, 3.

[50] Y. Jung, W. Lee, K. Jung, B. Park, J. Park, J. Ko, H. Cho, *Polymers* **2020**, *12*, 1412.

[51] F. Gaudière, I. Masson, S. Morin-Grognet, O. Thoumire, J.-P. Vannier, H. Atmani, G. Ladam, B. Labat, *Soft Matter* **2012**, *8*, 8327.